Numerical analysis of concrete block masonry beams under three point bending

Vladimir G. Haach[1]
Graça Vasconcelos[2]
Paulo B. Lourenço[3]

Abstract. A parametrical study of masonry beams through numerical modelling has been performed in order to better understand the mechanical behaviour of these elements. Boundary conditions, geometry and reinforcement ratios are the main parameters analysed in this study. The numerical simulation is performed with DIANA® software, based on the Finite Elements Method. A comparison between numerical and experimental results is presented in order to validate the simulation. In conclusion, it was verified that the behaviour of masonry beams is greatly affected by the boundary conditions and geometry, as expected. With regard to reinforcement, it was noted that horizontal reinforcement increases the flexural strength of beams. On the other hand, variation in horizontal reinforcement had no influence on the shear resistance of masonry beams. Finally, the combination of horizontal and vertical reinforcement is shown to enhance the flexural and shear behaviour of masonry beams.

Key words: masonry beams, shear, flexure, numerical modelling.

1 – Professor, University of Sao Paulo, Department of Structures, Av. Trabalhador Saocarlense, 400, 13566-590, Sao Paulo - SP, BRAZIL, Phone: (+55) 16 33739455, Fax: (+55) 16 33739482, E-mail: vghaach@sc.usp.br
2 – Professor, ISISE, Department of Civil Engineering, University of Minho, Azurém, 4800-058 Guimarães, PORTUGAL, E-mail: graca@civil.uminho.pt
3 – Professor, ISISE, Department of Civil Engineering, University of Minho, Azurém, 4800-058 Guimarães, PORTUGAL, E-mail: pbl@civil.uminho.pt

Introduction

In masonry buildings, masonry beams are the structural elements responsible for the distribution of vertical loads over openings and they are subjected to shear and flexure stresses. According to several authors, their design can be performed using the ultimate strength design method similar to that used for reinforced concrete beams (Khalaf et al. [1], Hendry [2], Drysdale et al. [3], Taly [4]). Nevertheless, the usual presence of cores in units and the anisotropy of masonry, generated mainly by mortar joints which are planes of weakness, make the behaviour of masonry beams more complex. In spite of Eurocode 6 [5] provides the design of masonry beams under flexure and shear, by applying classic formulations used for homogeneous materials, very limited experimental and numerical information is available in literature about the resisting mechanisms characterising the behaviour of masonry beams under in-plane shear and bending.

Based on experimental research carried out on masonry beams with variable depth to length ratios and variable tensile reinforcement ratios, Khalaf et al. [1] confirmed the assumption that plane sections remain plane during bending and obtained an ultimate compressive strain for masonry of about 0.003. Truss type reinforcement in bed joints was used by Limón et al. [6] in brick masonry beams (span to depth ratio equal to 4.5), which analysed the influence of the depth of the neutral axis, the quantity of reinforcement and the overlap of bars. By comparing the experimental and analytical results on the flexural strength it was found that diagonal bars appear to contribute to the flexural resistance of brick masonry beams. According to Jang and Hart [7] and Adell et al. [8] uniform distribution of longitudinal reinforcement leads to increasing of shear resistance by dowel action. Another important aspect regarding a section in

bending is its compressive strength, which can play a significant role in the resisting moment (Chen et al. [9]). Note that in the case of masonry beams compressive stresses act in the direction parallel to the bed joints.

Besides experimental analysis, numerical modelling of masonry beams can provide additional information on flexural and shear behaviour by considering the effect on some parameters. Variables such as geometry, boundary conditions and variation of vertical and horizontal reinforcement can be easily evaluated after the appropriate validation of the numerical model.

In recent years some numerical approaches have been developed, from which an enhanced understanding of the mechanical behaviour of masonry has been achieved. There are two numerical approaches that have been adopted by researchers for numerical analysis of masonry structures, namely macro-modelling and micro-modelling. It is well-known that both approaches reproduce satisfactorily the behaviour of masonry structures, having specific and particular applications. In the macro-modelling approach, masonry is considered as a homogeneous material and the constitutive models represent the average material properties of masonry as a composite material. Several studies have been developed for the derivation of the homogenized elastic properties of the smeared masonry continuum (Anthoine [10], Lee et al. [11]) and for the representation of the inelastic behaviour of masonry (Lourenço [12], Luciano and Sacco [13], Zucchini and Lourenço [14], Shieh-Beygi and Pietruszczak [15], Reyes et al. [16]).

In the case of micro-modelling, the masonry material is considered as a discontinuous assembly of units connected by joint interfaces simulated by appropriate constitutive laws. Micro-models are usually applicable to small size structures where

detailed analysis on the resisting mechanisms and failure modes are to be evaluated (Lotfi and Shing [17], Lourenço [12], Giambanco et al. [18], Oliveira and Lourenço [19], Alfano and Sacco [20]). The great advantage of micro-modelling is the capacity for detecting local crack patterns and local failures. Lourenço and Rots [21] proposed a powerful interface cap model based on modern plasticity concepts, capable of capturing all masonry failure mechanisms, namely tensile cracking, frictional slip and crushing along interfaces

Giambanco and Di Gati [22] and Giambanco et al. [18] proposed a simplified, elastoplastic interface model addressing the cohesive-frictional joint transition by taking into account geometrical dilatancy related to the roughness of fracture-slip surfaces appearing in the pure frictional stage. The yield surface adopted is expressed by a classical bilinear Coulomb condition with a tension cut-off. More recently Chaimoon and Attard [23] proposed an elastoplastic interface model for masonry structures. The tensile and shear behaviour of joints is represented by a tension cut-off and a Coulomb failure surface, whereas the compressive behaviour is described by a linear cap surface. This model has been applied in the analysis of masonry beams under in-plane three-point bending tests (Chaimoon and Attard [24]). A good agreement between the experimental and numerical results, in terms of load-displacement diagrams and failure modes in three point bending tests, was found. The fracture process in masonry beams involved both tensile and shear fracture along the vertical and horizontal bed joints.

Aiming at better understanding the resisting mechanisms of concrete block masonry beams, used above openings in the case of modern masonry buildings, it was decided to perform a parametric study based on numerical analysis, taking into account the geometry of masonry beams, boundary conditions and vertical and horizontal

reinforcement ratios. The numerical model was based on a micro-modelling approach so that the resisting mechanism, mainly at the level of unit-mortar interfaces, could be acquired. The calibration of the numerical model was based on experimental results of an extensive experimental investigation, also taking into account the mechanical properties resulting from the mechanical characterisation of concrete block masonry.

Brief description of experimental tests

The calibration of the numerical model was carried out from the experimental results obtained from flexural and shear tests performed on masonry beams built with concrete block units (Haach [25]). The static monotonic tests were carried out following two typical test setups (three and four point load configurations) recommended by EN846-9 [27], see Fig. 1. Two and three cell hollow blocks were used in the construction of the masonry beams, leading to two masonry bonds, namely beams with filled vertical joints (two hollow cell blocks) and beams with unfilled (dry) vertical joints (three cell hollow blocks). Fourteen masonry beams, of dimensions 1224mm length, 400mm depth and 100mm thickness, were tested under a four point bending configuration. Ten masonry beams, of 600mm length, 400mm depth and 100mm thickness, were tested under a three point configuration. Truss-type pre-fabricated reinforcement was used for both bed and head joints. A summary of the typologies of the masonry beams is shown in Table 1. Here, F denotes flexure, S denotes shear, 2C and 3C relates to the type of unit (two and three cell hollow blocks respectively) and UM means unreinforced masonry. The diameter and ratio of the horizontal and vertical reinforcement are denoted by ϕ_h and ϕ_v, ρ_h and ρ_v, respectively The designations D3 and D5 are related to the diameter of the bed joint reinforcement in the case of the

bending specimens. The letter C indicates that the bending specimen beams have bed joint reinforcement only at first course (from the bottom), and the letter D indicates that bed joint reinforcement is uniformly distributed in depth. In the case of masonry beams tested under a three load configuration, SH means that masonry beams only have horizontal reinforcement, and S1, S2 and S3 indicate vertical reinforcement ratios.

In case of F-specimens, two vertical reinforcement bars of 5mm in diameter were introduced at the vertical cores of the concrete blocks between the supports and the load application points to avoid shear failure at the supports. Two vertical reinforcement bars were added at mid-span (indicated with M) in order to assess their contribution to the flexural behaviour of the beams, such as an increase in the flexural strength and the prevention of vertical splitting stresses developed at the upper compressive region due to high compressive stresses.

In the case of beams under three load configuration tests, traditional steel bars (ρ_h = 0.70%) were positioned in a layer of mortar at the base of the beam and bed joint reinforcement was added at all courses. It should be pointed out that the position of the vertical reinforcement was, to a certain extent, defined by the geometry of the concrete units and their perforation.

Horizontal and vertical reinforcement ratios, ρ_h and ρ_v, and the distribution of reinforcement were the main parameters analysed in the experimental investigation. A more detailed overview of the experimental results can be found in Haach [26].

Numerical modelling

The numerical model applied to study reinforced concrete block masonry under in-plane loading was defined using the software DIANA® [28]. The micro-modeling

approach was chosen for the simulation since it includes all the basic failure mechanisms that characterize masonry, enabling the detailed representation of resisting mechanisms of the masonry beams. The Newton-Raphson iteration procedure was used with displacement control, and an energy convergence criterion with a tolerance of 10^{-3} was adopted. After validation, the numerical model will be used for a parametric study to further assess the influence of parameters on the flexural and shear behaviour of concrete block masonry beams.

Finite element mesh and boundary conditions

For the numerical simulation a simplified micro-modelling approach was adopted. Thus, the finite element mesh was composed of continuum and interface elements to represent the masonry units and the masonry joints, respectively, see Fig. 2. In the case of concrete units, eight-node isoparametric plane-stress elements with a 2×2 Gauss integration scheme were adopted. Aimed at foreseeing possible cracking passing through the units, potential vertical cracks were introduced at mid-length of the units. For the joints, six node interface elements with zero thickness and a 3-point Lobatto integration scheme were considered.

Reinforcement was modelled through embedded bars, resulting in a slight increase in the stiffness of the finite element model. Reinforcement strains were computed from the displacement field of the continuum elements, which implies a perfect bond between the reinforcement and the surrounding material.

When considered as an integral part of a structural masonry building, masonry beams present an intermediate behaviour between a beam restrained in both ends and a simply supported beam. The boundary conditions take a central role in the behaviour of masonry beams as they govern the failure mechanism. Depending on the boundary

conditions of the beams, flexural or shear effects can prevail. Due to the difficulty of simulating restrained ends in the laboratory, it was decided to consider only simply supported beams in the research experimental program. The simply supported masonry beams tested in the laboratory were used to calibrate the numerical model but the parametric study also considered the possibility of having fixed ends so that the boundary conditions could be evaluated in relation to the in-plane shear and flexural behaviour of the beams.

Material models and mechanical properties

Following the micro-modelling approach, where all materials of the reinforced concrete block masonry beams with mechanical nature are independently modelled, also different materials models were used, namely to represent the mechanical behaviour of reinforcement, units, vertical and horizontal unit-mortar interfaces and the potential cracks in the middle of units. Most of the mechanical properties for the description of the material models were obtained through experimental tests on materials and masonry assemblages from Haach [26].

The non-linear behaviour of the concrete masonry units was represented by a Total Strain Crack Model based on a fixed stress-strain law concept available in the commercial software DIANA® [28]. The tensile and compressive behaviour of the material is represented with one stress-strain relationship in a coordinate system that is fixed upon crack initiation. Exponential and parabolic constitutive laws were used to describe the tensile and compressive behaviour of the concrete masonry units respectively. The mechanical properties needed to describe this material model are the elastic modulus of concrete units (E = 9.57 GPa), the Poisson's ratio of concrete units (ν

= 0.20), the tensile and compressive strength of concrete units (f_{tu} = 3.19 MPa and f_{cu} = 12.13 MPa, respectively), the fracture energy of units under tension and compression (G_{fu}^{I} = 0.06 N/mm and G_{cu} = 10.00 N/mm, respectively) and the shear retention factor (β = 0.01). Due to the impossibility of obtaining the post-peak behaviour in tension and compression of the three cell concrete units, the values of fracture energy, both in tension and compression, were obtained from the experimental results obtained by Mohamad [29] in concrete blocks with similar raw material composition.

An interface cap model with modern plasticity concepts proposed by Lourenço and Rots [21], and further enhanced by Van Zijl [30], was used for interface elements describing the masonry joints. The interface material model is appropriate to simulate fracture, frictional slip as well as crushing along material interfaces, which are the possible failure modes of the masonry unit-mortar interfaces. The model requires the elastic normal and transverse stiffness of bed joints (k_n = 20 N/mm^3 and k_s = 48 N/mm^3, respectively). The normal stiffness was calculated based on the results of the direct tensile tests carried out to characterise the tensile bond strength of the unit-mortar interface (Vasconcelos et al. [31]). The shear stiffness was obtained from the results of shear tests carried out on triplet specimens to characterise the shear behaviour of the concrete unit-mortar interface (Haach [25]). The yield function with exponential softening for the tension cut-off model requires the tensile bond strength of bed joints (f_t = 0.33 MPa) and the mode I fracture energy (G_f^I = 0.017 N/mm). The bond tensile strength was obtained from the experimental results of flexural tests of masonry carried out in the direction parallel to bed joints (Haach [25]). Due to the difficulty of obtaining mode I fracture energy of the unit-mortar interface, this mechanical property was

defined by fitting numerical and experimental results obtained in the masonry walls (Haach [25]).

The behaviour of the masonry material in compression is modelled by a constitutive law composed by a parabolic hardening rule and a parabolic exponential softening branch (Lourenço and Rots [21]). For the definition of this constitutive law the value of compressive strength (f_c = 5.95MPa) and the compressive fracture energy (G_c = 5.00 N/mm) are needed. These mechanical properties were obtained from uniaxial compressive tests carried out on masonry wallets. Additionally, the parameter C_{ss} needed to take into account the contribution of shear stress to compressive failure (C_{ss} = 5.3), was defined by fitting the numerical to experimental results obtained in the masonry walls (Haach [25]).

The shear behaviour of the unit-mortar interfaces is given by the Coulomb failure criterion. All mechanical parameters defining the Coulomb type failure criterion were obtained from the tests carried out on triplet specimens (Haach [25]). The definition of this function is made through consideration of cohesion (c = 0.42 MPa), friction coefficient (μ = 0.49), dilatancy coefficient ($tan\psi$ = 0.52) and the shear fracture energy (G_f^{II} = 2.0 N/mm). In order to capture cohesion softening and friction softening a residual friction coefficient (μ_{res} = 0.43) was also considered. In the model, the dilatancy is considered to be dependent on the normal confining stress and on the shear slipping. Thus, for the correct definition of the dilatancy the confining normal stress at which the dilatancy becomes zero (σ_u = 1.35 MPa) and the dilatancy shear slip degradation coefficient (δ = 1.64) were also obtained by experimental analysis.

In the case of the dry vertical joints, the shear behaviour was also modelled based on the Coulomb criterion, with null cohesion and a friction coefficient corresponding to

the dry contact between two surfaces of concrete (μ = 0,65). Very low values of normal and transverse stiffness (2 N/mm^3) were considered, with zero tensile strength.

According to Lourenço and Rots [21] it is useful to model potential cracks in units in order to avoid an overestimation of the collapse load and of the stiffness. Thus, potential cracks placed in the middle of the units were considered through interface elements with a discrete cracking model. High stiffness should be considered for these interfaces according to the suggestion of Lourenço [12] (k_n = 10^6 N/mm^3 and k_s = 10^6 N/mm^3, respectively). In addition, an exponential softening behaviour was adopted for the tensile behaviour of these interfaces with a tensile bond strength, f_t, of 3.19 MPa and a mode I fracture energy, G_f^I, of 0.06 N/mm. These properties were obtained from uniaxial compressive tests carried out on the concrete units (Haach [25]). The constitutive law for discrete cracking in DIANA® [28] expresses the stresses as a function of the total relative displacements between surfaces.

An elasto-plastic model based on the yield criterion of Von Mises was adopted to describe the behaviour of the reinforcement considering the yield stress equal to 580 MPa and the Young's modulus equal to 196 GPa. These properties were obtained from tensile tests carried out on reinforcements (Haach [25]). As the reinforcement elements overlap the interface elements representing the masonry joints, and thus have traction components in the same directions as the interface elements (normal and shear components), a 'free length' (thickness of the joints) is needed in order to properly account for the stiffness of the interface crossed by the reinforcement. Reinforcement considerably increases the stiffness of the interface elements and the additional normal and shear stiffness of the interface elements crossed by the steel reinforcements is given respectively by Eq. 1 and Eq. 2:

$$k_n = \frac{E_s}{l_{fr}} \tag{1}$$

$$k_s = k_t = \frac{E_s}{2l_{fr}} \tag{2}$$

where, E_s is the elastic modulus of reinforcements and l_{fr} is the thickness of mortar joints.

It should be stressed that the presence of reinforcement leads to a significant increase of the elastic stiffness of the interfaces. As the stiffness attributed to the interfaces is much larger than the stiffness attributed to the masonry joint, the global non-linear problem becomes ill-conditioned. The number of iterations needed to achieve convergence, and consequently the computational effort, increase.

Validation of numerical model

By comparing the experimental and numerical results in terms of maximum load applied to the types of masonry beams summarised in Table 2, it is observed that the numerical analysis provides reasonable agreement for the majority of the masonry beams, with a difference between experimental and numerical ultimate load lower than 15%. The higher differences are obtained for unreinforced specimens (F-3C-UM, F-2C-UM). The failure modes obtained for the unreinforced masonry are initiated by a central vertical joint and progresses to the top of the beams through the horizontal and vertical joints in a stair stepped configuration. This failure pattern involves mainly tensile and shear bond resisting mechanisms at the unit-mortar interface level, in agreement with the results reported by Chaimoon and Attard [24]. Thus, the shear strength parameters like cohesion and friction angle take a major role in the behaviour of these beams. On

the other hand, it should be mentioned that the mortar used in the construction of the unreinforced specimens exhibited lower values of compressive strength, which indicated that, possibly, the adherence was not as good as the one obtained in the triplet test and used in the numerical modelling. It is likely that the influence of cohesion is not much relevant in the case of specimens combining horizontal and vertical reinforcement.

The comparison of selected numerical and experimental load-displacement diagrams, obtained from the LVDT placed at mid length of the beams, for both load configurations and for masonry beams built with 3C- and 2C-units is displayed in Fig. 3. It can be observed that specimens under the four point load configuration exhibit a typical flexural behaviour presenting reasonable agreement in the pre-peak regime with numerical model. Lesser agreement between experimental and numerical responses was observed in specimens governed by shear failure patterns (F-3C-D5-D-M and F-2C-D5-D-M). In fact, it can be seen that the increase in the horizontal reinforcement ratio leads to a change in the cracking patterns from flexure to shear.

In the case of S- specimens (three point load configuration) there was a very good agreement of numerical and experimental load-displacement diagrams for specimens failing in shear for the pre-peak and post-peak regime. The specimen S-2C-SH, in which only horizontal reinforcement was added, exhibited the worst agreement both in terms of ultimate load and pre-peak regime due to the local crushing failure under the load application point that occurred in this test.

It should be highlighted that numerical and experimental cracking patterns and failure modes showed very reasonable agreement. In the case of F- specimens, flexural stair stepped cracks growing from the vertical joints at the mid-span of the masonry

beams up to the upper edge of the beams were observed in the numerical model, similarly to the crack patterns observed in the experimental specimens, see Fig. 4a. In case of S- specimens the numerical model also reproduces very well the localisation of the diagonal strut crushing according to that observed in experimental tests, see Fig. 4b.In addition, it should be mentioned that the numerical model predicts very well the experimental strains developed in the reinforcement. As an example, Fig. 5 shows excellent agreement between the numerical and experimental strains at bed joint reinforcements (flexural specimen F-3C-D5-D) along the depth of the beam.

To sum up, it is stressed that, in general, a reasonable agreement was achieved between numerical and experimental results obtained in masonry beams. Due to the simplifications considered, numerical modelling was not able to capture the cracking of the webs of the units observed in experiments due to the high compression stresses at the upper region of the beams. However, it is considered that the numerical model is acceptable to carry out the parametric study.

Parametric study

The main aim of the parametric study was to assess the influence of some parameters, which could not be evaluated in the experimental investigation both in relation to in-plane flexural and shear behaviour of masonry beams. The parameters selected were (i) the span to depth ratio, (ii) the horizontal reinforcement ratio and (iii) the combination of vertical and horizontal reinforcement. These parameters were evaluated for two boundary conditions, namely simply supported and fixed end masonry beams, in order to discuss their role when flexure and shear failure predominated. For each boundary

condition eight span to depth ratios were adopted, as shown in Fig. 6 and Fig. 7 (for simply supported beams). The same geometries were used for fixed end beams, leading to slightly lower depth to span ratios due to the location of the supports. A three point load configuration was adopted for the numerical simulation. The application of the load was in displacement control in order to avoid convergence problems in the post-peak regime. The parametric study was carried out by considering the material properties and the three cell units used in the calibration of the numerical model.

Analysis 1- Influence of the geometry of the unreinforced beams

Similarly to what was found in the experimental analysis, it was observed that unreinforced masonry beams behaved in a very brittle manner due to the low strength of the unit-mortar interfaces. The crack patterns depended on the predominant shear or flexural behaviour but always followed the unit-mortar interfaces.

Simply supported masonry beams failed in flexure, whereas fixed end beams failed in shear. Fig. 8 shows the typical cracking found for both boundary conditions under consideration. The onset of flexural cracking occurred at the bottom vertical joints located at mid span, where tensile normal stresses in vertical joints were at maximum, see Fig 10a. The shear cracking pattern was characterized by diagonal cracking along the compressed struts following the unit-mortar interfaces, see Fig. 8b. In both cases, the strength of beams was controlled by the shear and tensile bond strength of the vertical and horizontal bed joints. It is noted that the tensile bond strength of the dry vertical joints is zero, meaning that the progress of the flexural cracks from the bottom to the top of the beams was due to the shear bond strength failure of the bed joints. This means also that the flexural strength of masonry beams

with dry head joints is assured by the shear strength of the bed joints. On the other hand, the shear bond strength was dependent on the normal stresses of the bed joints. The profiles of normal stresses at the bed joint of the first course (from the bottom) of simply supported beams with different span to depth ratios are shown in Fig. 9. For the same depth and increasing span length corresponding to a higher span to depth ratio, the normal stresses present higher amplitude. This means that normal stresses in bed joints increase with the higher flexural deformed shape resulting in the greater interlocking between units. This behaviour is also valid in the case where the depth increases and the span length is kept constant, where the interlocking between units progressively decreases as a result of the lower flexural deformation of the beams.

In the case where shear stresses predominate over flexural stresses (all fixed end masonry beams), it can be seen that the shear resistance of the beams depends on the combination of the tensile and shear bond strength of the mortar bed and dry head joints, respectively. Indeed, the progress of diagonal cracks depends on the achievement of the dry friction resistance of the head joints and on the tensile bond strength of the mortar joints, as the shear sliding of vertical joints induces tensile stresses at the mortar bed joints leading to diagonal cracking mostly at the unit-mortar interfaces. It should be noted that the shear friction resistance of the vertical joints is enhanced by the compressive stresses in the direction parallel to the bed joints developed in the upper region of the beam due to flexure.

As aforementioned, due to the low shear and tensile bond strength of the unit-mortar interface, diagonal cracking mostly develops along the unit-mortar interfaces. This means that the shear behaviour of masonry beams is very dependent on the normal stresses in the vertical and horizontal joints, since it is assumed that their shear

resistance follows a typical Mohr-Coulomb criterion. From Fig. 10, where the distribution of normal and shear stresses along the diagonal crack is shown (vertical interfaces), it can be observed that the normal stresses present higher values at the extremities of the diagonal crack line (DCL) resulting from the typical normal stress diagram due to bending moments. It can be noted that the evolution of normal stresses along the diagonal considers different vertical alignments, resulting in a non-symmetric normal stress distribution. In the middle of the DCL normal stresses present low values which lead to a minimum shear strength. By comparing the normal stresses through the DCL among the masonry beams with different depths and spans for a same load level it can be concluded that the normal stresses increase with the reduction of depth of the beam and with the increase of the span of the beam, see Fig. 11. The normal stresses along the depth of the masonry beams can be the result of axial forces and bending moments. The increase in the normal stresses along the DCL is the result of: (a) an increase in the bending moments in the case of increasing span lengths; (b) the reduction of the inertia moment of the cross section in case of the decrease on the depth of the masonry beams.

The results obtained from the distribution of shear stresses along the DCL reveals that they also increase with the reduction of beam depth and with the increase of the beam span, see Fig. 12. In the first case it is expected that the shear stresses decrease with an increase of beam depth, since the length on which the shear stresses develop for the same load level increases. The increasing shear stresses with increasing beam span lengths can be explained in a similar manner. In the case of increasing span-to-depth ratio, it is possible that the damage at the bottom of the beam due to flexure, associated

with higher bending moments, reduces the effective depth resisting to shear stresses leading to the higher shear concentration stresses.

By comparing the progress of the vertical load applied to the masonry beams with the span to depth ratio illustrated in Fig. 13, it can be seen that the span to depth ratio plays a major role on the maximum load applied to the beams. The resistance of fixed end beams is clearly higher than the resistance of simply supported beams. In both cases, the increase in the span to depth ratio results in the decrease of the resistance of the masonry beams. However, the reduction of the resistance is particularly remarkable when the depth of the cross section is reduced, whereas the influence of the increase on the span length keeping the cross section constant is much less relevant. In fact, a decrease in the depth of the beam results in a reduction of the resisting cross section and in the resisting geometric properties like inertia moment, leading to a lower capacity to resist bending and shear stresses. Besides, as aforementioned, for the same load acting on the beam the shear stresses are minimal for the highest depth of the beam, meaning that extra load can be applied before failure is reached.

The reduction of the resistance for increasing span lengths is essentially associated to an increase in the bending moments and higher stress concentrations. In the case of fixed end masonry beams, where the shear response is predominant, an increase in the normal stresses for increasing span lengths, leading to an increase in the shear strength along the interfaces, appears to be counterbalanced by an increase in the bending moment. In relation to fixed end masonry beams the higher resistance of the beam with a span to depth ratio (L/H) of 2.03 can also be explained by its geometry, which completely avoids the sliding of the central region over the diagonal crack of the

beam, as the progress of the diagonal crack from the top of the beam is restrained by the supports.

Analysis 2 – Assessment of the influence of the horizontal reinforcement

The influence of the horizontal reinforcement in the flexural and shear behaviour of masonry beams was analysed by considering different arrangements of bed joint reinforcement for both boundary conditions. Two different arrangements of reinforcement were considered: (i) reinforcement uniformly distributed along the depth and (ii) reinforcement concentrated at first course. Three horizontal reinforcement ratios, ρ_h, were considered: 0.10%, 0.20% and 0.30% in the case of uniform distribution along the depth and one reinforcement ratio equal to 0.10% was considered in the case of concentrated bed joint reinforcement at first course.

The variation of the load capacity of simply supported and fixed end masonry beams for different depth to span length ratios is displayed in Fig. 14. As expected, addition of horizontal reinforcement results in the improvement of flexural resistance due to the enhancement of the tensile strength of masonry and avoids its premature and brittle failure. Simply supported masonry beams with horizontal reinforcement concentrated at the first bed joint exhibited higher flexural strength, as expected, since the contribution for the improvement of the tensile strength is higher due to the higher reinforcement area with a higher lever arm. In general, the load capacity of beams was clearly improved by the introduction of horizontal reinforcement, but the variation of the horizontal reinforcement ratio seemed not to influence the strength of masonry beams. The increase of the load capacity was more remarkable in simply supported beams, achieving in average 50% higher values than in unreinforced masonry beams,

probably due to the change in failure mode. In the case of fixed end beams, shear failure mode with diagonal cracking is maintained and an increase in the load capacity of 15% is attained.

In the case of fixed end masonry beams, whose predominant shear behaviour is revealed by the shear diagonal cracking, it should be noted that the concentration of bed joint reinforcement at first course (from the bottom) appears to be harmful. This means that a concentration of bed joint reinforcement should be avoided. The concentrated reinforcement at the first course (from the bottom) is not effective in the distribution of cracking, even if it avoids flexural cracking at the bottom edge of the beam leading to shear failure with diagonal cracking. A more distributed crack pattern is only achieved through the distribution of reinforcement along the depth of the beam. The increase on the reinforcement ratio also improves the cracking distribution.

From the distribution of normal and shear stresses along the DCL for the same load level it can be concluded that the introduction of horizontal reinforcement reduces the level of stresses in the DCL, independently on the boundary condition. The lowering of the stresses along the DCL is the result of the stress transfer between the masonry and reinforcement. The reduction of normal and shear stresses is related to the arrangement of the steel bars along the depth of the masonry beam. The level of shear stresses in unreinforced and reinforced masonry beams with concentration of bed joint reinforcement at first course (from the bottom) is practically coincident. This behaviour confirms that the concentrated reinforcement is not effective in the redistribution of shear stresses between masonry and reinforcement, meaning that horizontal reinforcement did not provided an increase in the shear capacity of masonry beams.

Analysis 3 – Evaluation of the contribution of combined vertical and horizontal reinforcement

The influence of vertical reinforcement in the behaviour of masonry beams was analysed by considering three vertical reinforcement ratios, namely 0.05%, 0.15% and 0.25% and keeping a constant bed joint reinforcement ratio of 0.20%. The vertical reinforcement spacing was fixed in 200mm, even if for the vertical reinforcement ratio of 0.05% an additional spacing of 300mm was considered. In this analysis the same geometry, loading and boundary conditions of the previous studies were used.

Figure 17 shows the progress of the maximum load with the variation of the span to depth ratio and with the variation of the vertical reinforcement ratio. It can be observed that the maximum load increases significantly with the addition of vertical reinforcement. Besides, vertical reinforcement controls the opening of diagonal cracking.

In case of simply supported masonry beams, it can be observed that the variation of the vertical reinforcement ratio has no significant influence on their behaviour, which can be explained by the crushing failure mode of the beams at the top. Simply supported beams with large span length to depth ratios, such as the beam with L/H = 4.57, reached the crushing of masonry before the yield of reinforcement. The strength of beams increased with the decrease of the span to depth ratio and the crushing took place after the yielding of reinforcement. In fact, with the increase of the applied vertical load some vertical reinforcement reached the yield stress, which means that the beam became more deformable. This enabled also the yielding of horizontal reinforcement, contributing to the increase of the ultimate load of the beams.

In the case of fixed end masonry beams, given the preponderance of diagonal cracking over flexural cracking, the vertical reinforcement was effective in the resistance to shear stresses, always achieving the yield strength. As in the case of simply supported beams, the yield of vertical reinforcement made the beam more deformable, leading to the yielding of horizontal reinforcement and finally to the crushing of masonry. Therefore, the increase in the vertical reinforcement ratio delayed the crushing of masonry and improved the behaviour of the beam.

Variation in spacing of vertical reinforcement did not influence the behaviour of simply supported masonry beams, but in case of fixed end specimens higher spacing in general appeared to reduce the strength of the beams. This behaviour can possibly be explained by the higher capacity of control over the opening of diagonal cracks and premature crushing of masonry, see Fig. 16. In contrast to the simply supported beams, in fixed end masonry beams an increase in the vertical reinforcement ratio improves the shear capacity of the beams, confirming its effective role in resisting shear stresses.

Finally, it was decided to evaluate the influence of the horizontal reinforcement ratio by keeping the configuration of vertical reinforcement. For this, a constant vertical reinforcement ratio of 0.05% with a spacing of 200mm was considered. Three horizontal reinforcement ratios were adopted with uniform distributed reinforcement along depth of the beams, namely 0.10%, 0.20%, 0.30% and one reinforcement ratio of 0.10% was considered when concentrated horizontal reinforced was introduced at first course.

From Fig. 17, it can be seen that the introduction of vertical reinforcement improved the contribution of the horizontal reinforcement ratio to the strength of the beams. In fact, as aforementioned, without vertical reinforcement the behaviour of the

simply supported beams was almost not affected by the variation of the horizontal reinforcement ratio. This behaviour is valid for all span to depth ratios.

In fixed end masonry beams, similarly to the discussion when only horizontal reinforcement was introduced to the beams, their behaviour shows practically no sensitivity to the variation of the horizontal reinforcement ratio. However, it should be mentioned that the addition of vertical reinforcement enhances the load capacity when results are compared to the values obtained in beams reinforced only at bed joints. This means that in the masonry beams governed by shear the horizontal reinforcement does not seem to influence in a great extent the shear strength of masonry beams.

Conclusions and final remarks

For the numerical simulation of concrete block masonry beams under flexure and shear a micro-modelling approach was adopted due to the need to understand in detail the resisting mechanisms. In a first phase the numerical model was calibrated based on the experimental results of masonry beams tested under four point and three point load configurations. The mechanical properties of materials used in the model were obtained from experimental tests, even if a few of them had to be obtained by a comparison of the numerical and the experimental results. Very reasonable agreement was found between the numerical force-displacement diagrams describing the mechanical behaviour of masonry beams. In a second phase, an extensive parametric study was performed aiming at evaluating the influence of the different parameters such as the aspect ratio, boundary conditions and horizontal and vertical reinforcement ratios in the behaviour of masonry beams.

The parametric study carried out on masonry beams revealed that:

(a) The mechanical behaviour of unreinforced masonry beams appeared to be controlled by tensile and shear bond resisting mechanisms as flexural and diagonal cracks developed along the unit-mortar interfaces. Unreinforced masonry beams presented very brittle behaviour.

(b) Horizontal reinforcement increased the flexural strength of masonry beams and improved ductility. However, it should be stressed that the enhancement on strength was more remarkable in the case of simply supported beams, where flexural behaviour is predominant. Horizontal reinforcement increased the shear strength of masonry beams relative to unreinforced beams due to the prevention of sliding and thus of the progress of diagonal cracking.

(c) The sensitivity to variation of the bed joint reinforcement ratio is clear in the case where vertical reinforcement was added for simply supported beams. In case of fixed end masonry beams, the presence of horizontal reinforcement also contributes to the improvement of the strength of the beams but the strength was not sensitive to the variation of the reinforcement ratio.

(d) The introduction of vertical reinforcement combined with bed joint reinforcement improved considerably the flexural and shear resistance of masonry beams. The vertical reinforcements controlled the crack opening and generated a change in the failure mode of the beams promoting the crushing of masonry after yielding of vertical and bed joint reinforcement. It should be stressed that fixed end masonry beams were sensitive to the vertical reinforcement ratio, as it effectively contributed to improve the shear strength of the masonry.

Acknowledgements

This work was in part supported by a contract from DISWall – “Development of innovative systems for reinforced masonry walls” – (COOP-CT-2005-018120) awarded by the European Commission. The first author was supported by the Programme Alβan, the European Union Programme of High Level Scholarships for Latin America, Scholarship nº E06D100148BR.

References

[1] Khalaf, F. M., Glanville, J. I. & El Shahawi, M. (1983), “A study of flexure in reinforced masonry beams”, *Concrete International*, 5(6), pp.46-53.

[2] Hendry, A. W. (1998), *Structural Masonry*, MacMillan Press LTDA, London, UK.

[3] Drysdale, R. G., Hamid, A. A. & Baker, L. R. (1999), *Masonry structures: behaviour and design*, The Masonry Society, Boulder, Colorado, USA.

[4] Taly, N. (2001), *Design of reinforced masonry structures*, McGraw-Hill, New York, USA.

[5] EUROPEAN STANDARD. EN 1996-1-1 (2005), *Eurocode 6: Design of masonry structures. General rules for reinforced and unreinforced masonry structures*.

[6] Limón, T. G., Hortelano, A. M. & Fernández, B. M. (2000), “Vertical flexural behaviour of bed joint reinforced brick masonry”, *Proceeding of 12th International Brick and Block Masonry Conference*, Madrid, Spain.

[7] Jang, J. J. & Hart, G. C. (1995), “Analysis of concrete masonry beams”, *Journal of structural engineering*, 121(11), pp.1598-1602.

[8] Adell, J. M., Garcia-Santos, A., Lauret, B., López, C., Martín, H., Peña, J., Pol, M., Timperman, P. & Veja, S. (2008), “6m span beams tests on a new wall PI-brackets type”, *Proceedings of 14th International Brick/block Masonry Conference*, University of Newcastle, Australia, 10 p..

[9] Chen, Y., Ashour, A. F. & Garrity, S. W. (2008). “Moment/thrust interaction diagrams for reinforced masonry sections”, *Contruction and Building Materials*, 22(5), pp.763-770.

[10] Anthoine, A. (1995), “Derivation of in-plane elastic characteristics of masonry through homogenization theory”, *International Journal of Solids and Structures*, 32(2), pp.137-163.

[11] Lee, J. S., Pande, G. N., Midleton, J., Kralj, B. (1996), “Numerical modelling of brick masonry panels subjected to lateral loading”, *Computers and Structures*, 61(4), pp.735-745.

[12] Lourenço, P. B. (1996), *Computational strategies for masonry structures*, PhD Thesis, Delft University of technology, Delft, The Netherlands. Available from www.civil.uminho.pt/masonry.

[13] Luciano. R. & Sacco. E. (1997), “Homogenization technique and damage model for old masonry material”, *International Journal of Solids and Structures*, 34(4), pp.3191-3208.

[14] Zucchini, A. & Lourenço, P.B. (2009), “A micro-mechanical homogenisation model for masonry: Application to shear walls”, *International Journal of Solids and Structures*, 46, pp.871-886.

[15] Shieh-Beygy, B. & Pietruszczak, S. (2008), “Numerical analysis of structural masonry: mesoscale approach”, *Computers and Structures*, 86, pp.1958-1973.

[16] Reyes E., Gálvez, J. C., Casati, M .J., Cendón, D. A., Sanchio, J. M. & Planas, J. (2009), “An embedded cohesive crack model for finite element analysis of brick work masonry fracture”, *Engineering Fracture Mechanics*, 76, pp.1930-1944.

[17] Lotfi, H. R. & Shing, P. B. (1994), “Interface model applied for fracture masonry structures”, *Journal of Structural Engineering*, 120(1), pp.63.80.

[18] Giambanco, G., Rizzo, S. & Spallino, R. (2001), “Numerical analysis of masonry structures vis interface models”, *Computer Methods in Applied Mechanics and Engineering*, 190, pp.6493-6511.

[19] Oliveira, D .V. & Lourenço, P. B. (2004), “Implementation and validation of a constitutive model for the cyclic behaviour of interface elements, *Computers & Structures*, 82(17-19), pp.1451-1461.

[20] Alfano, G. & Sacco, E. (2006), “Combining interface damage and friction in a cohesive- zone model”, *International Journal of Numerical Methods in Engineering*, 68, pp.542-582.

[21] Lourenço, P. B & Rots, J. G. (1997), “Multisurface interface model for analysis of masonry structures”, *Journal of Engineering Mechanics*, 123(7), pp.660-668.

[22] Giambanco, G. & Di Gatti, L. (1997), “A cohesive interface model for the structural mechanics of block masonry”, *Mechanics Research Communications*, 24(5), pp.503-512.

[23] Chaimoon, K. & Attard, M. M. (2007), “Modeling of unreinforced masonry walls under shear and compression”, *Engineering Structures*, 29(9), pp.2056-2068.

[24] Chaimoon, K. & Attard, M. M. (2009), “Experimental and numerical investigation of masonry under three-point bending (in-plane)”, *Engineering Structures*, 31(1), pp.103-112.

[25] Haach, V.G., Vasconcelos, G., Lourenço, P.B. (2011), “Experimental analysis of reinforced concrete block masonry spandrels using pre-fabricated planar trussed bars”, *Construction and Building Materials* (in press).

[26] Haach, V.G. (2009), *Development of a design method for reinforced masonry subjected to in-plane loading based on experimental and numerical analysis*, PhD Thesis, University of Minho, Portugal.

[27] EUROPEAN STANDARD. EN 846-9 (2000), *Methods of tests for ancillary components for masonry. Part 9: Determination of flexural resistance and shear resistance of lintels*.

[28] DIANA® (2009), *Finite Element Analysis: User's Manual release 9.4*, TNO DIANA BV, Delft, The Netherlands.

[29] Mohamad, G. (2007), "*Mechanism failure of concrete block masonry under compression*", PhD Thesis, University of Minho, Portugal (In Portuguese). Available from www.civil.uminho.pt/masonry.

[30] Van Zijl, G. P. A. G. (2004), "Modeling masonry shear-compression: Role of Dilatancy highlighted", *Journal of engineering mechanics*, 30(11), pp.1289-1296.

[31] Vasconcelos, G., Lourenço, P.B., Haach, V.G. (2008). "Avaliação experimental da aderência de juntas de alvenaria de blocos de betão", *Proceedings of 7º Congresso Nacional de Mecânica Experimental*, Vila Real, Portugal, pp.101-103. (in Portuguese)

List of captions for illustrations

Fig. 1 – Test setup of masonry beams: (a) four point load test and (b) three point load test (dimensions in mm).

Fig. 2 – Example of mesh applied to the masonry beams.

Fig. 3 - Comparison between numerical and experimental results (Force vs. displacement diagrams): (a) F-3C-D3-C, (b) F-2C-D3-C, (c) S-3C-S3 and (d) S-2C-S3.

Fig. 4 - Comparison between numerical and experimental crack patterns: (a) F-3C-D3-C and (b) S-3C-S3.

Fig. 5 – Comparison between experimental and numerical strains in horizontal reinforcement of specimen F-3C-D5-D.

Fig. 6 – Simply supported masonry beams: variation of span.

Fig. 7 - Simply supported masonry beams: variation of depth.

Fig. 8 - Deformed mesh with the representation of the maximum principal stresses after the application of a displacement equal to 0.75 mm: (a) simply supported beam (L/H = 3.05) and (b) fixed end beams (L/H = 3.55).

Fig. 9 - Normal stress distribution in first bed joint of simply supported beams with the same level of loading: (a) variation of span length (P=2kN) and (b) variation of depth (P=5kN).

Fig. 10 - Profiles of stresses in vertical joints along the diagonal crack line (DCL) in fixed end beam (L/H = 4.06): (a) normal stresses and (b) shear stresses.

Fig. 11 - Normal stresses in vertical joints along the DCL of fixed end beams for the same level of vertical load: (a) influence of the variation of the depth (P= 10kN) and (b) influence of the variation of span (P= 5kN).

Fig. 12 - Shear stresses along vertical joints of the DCL of fixed end for the same level of vertical load: (a) influence of the variation of the depth (P= 10kN) and (b) influence of the variation of span (P= 5kN).

Fig. 13 - Variation of load capacity of unreinforced beams in relation to the span to depth ratio.

Fig. 14 – Variation of load capacity with variation of horizontal reinforcement ratio of beams reinforced only with horizontal bars: (a) simply supported and (b) fixed ends.

Fig. 15 – Variation of load capacity with variation of vertical reinforcement ratio of beams reinforced with vertical and horizontal bars: (a) simply supported and (b) fixed ends.

Fig. 16 – Deformed mesh with the representation of the minimum principal stresses after the application of a displacement equal to 3.00 mm in a fixed end beam with L/H = 3.36: (a) spacing equal to 200 mm and (b) spacing equal to 300 mm

Fig. 17 - Variation of load capacity with variation of horizontal reinforcement ratio of beams reinforced with vertical and horizontal bars: (a) simply supported and (b) fixed ends.

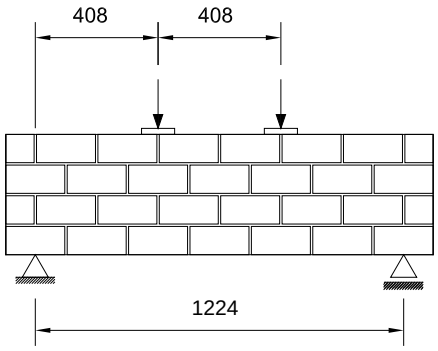

(a)

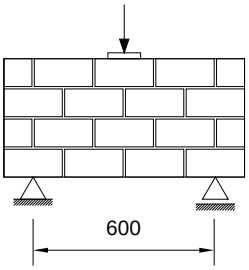

(b)

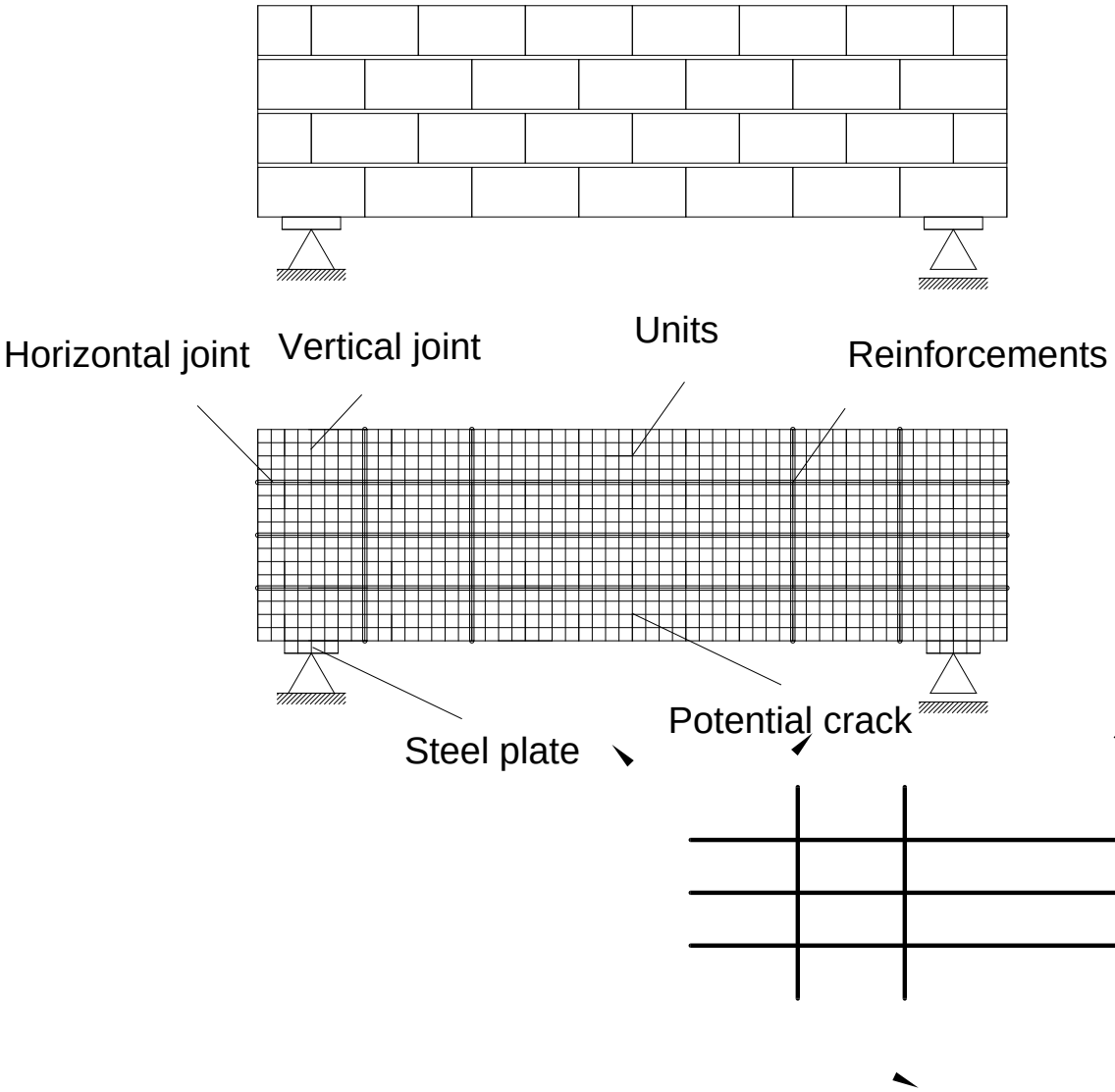
Horizontal joint
Vertical joint
Units
Reinforcements
Steel plate
Potential crack

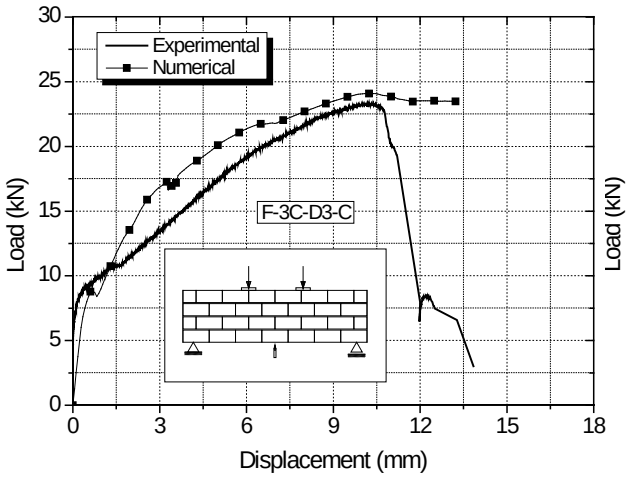
Experimental
Numerical
F-3C-D3-C
Load (kN)
Displacement (mm)
0
5
10
15
20
25
30
0
3
6
9
12
15
18

(a)

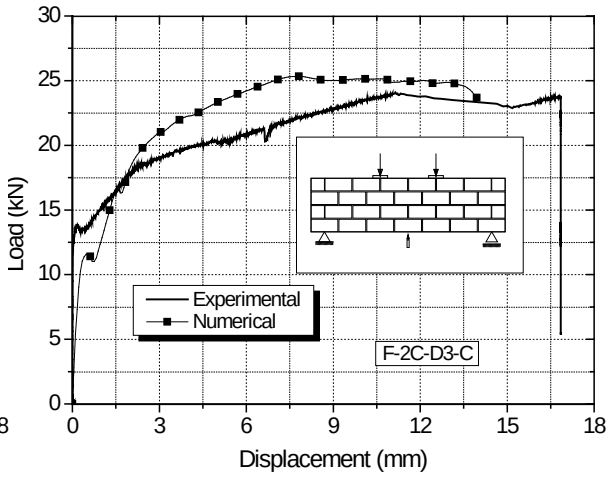
Experimental
Numerical
F-2C-D3-C
Load (kN)
Displacement (mm)
0
5
10
15
20
25
30
0
3
6
9
12
15
18

(b)

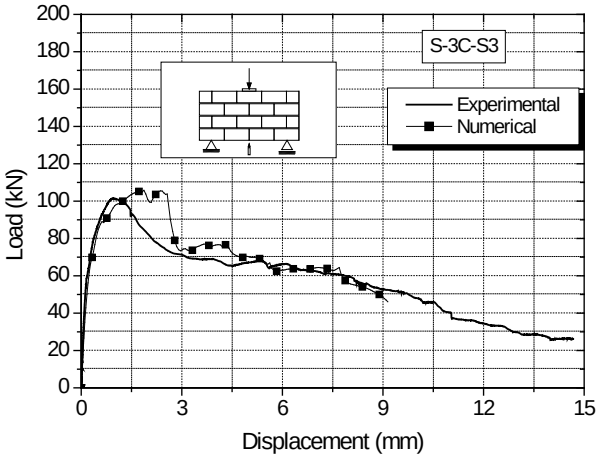
S-3C-S3
Experimental
Numerical
Load (kN)
Displacement (mm)
0
20
40
60
80
100
120
140
160
180
200
0
3
6
9
12
15

(c)

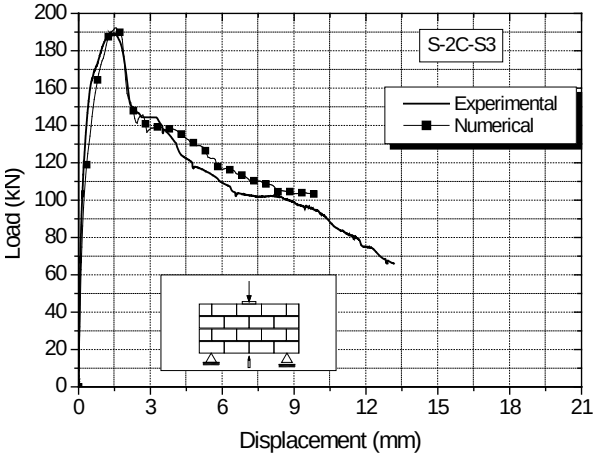
S-2C-S3
Experimental
Numerical
Load (kN)
Displacement (mm)
0
20
40
60
80
100
120
140
160
180
200
0
3
6
9
12
15
18
21

(d)

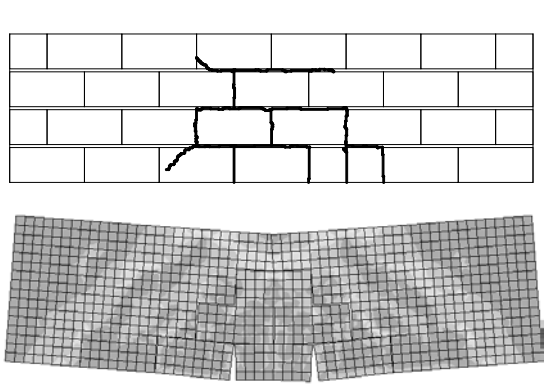

(a)

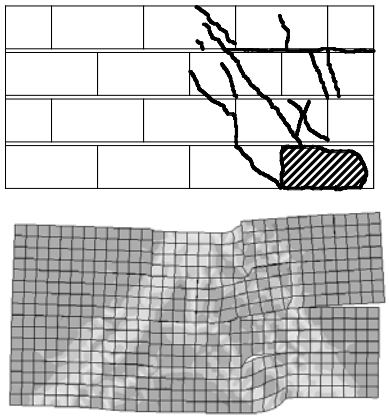

(b)

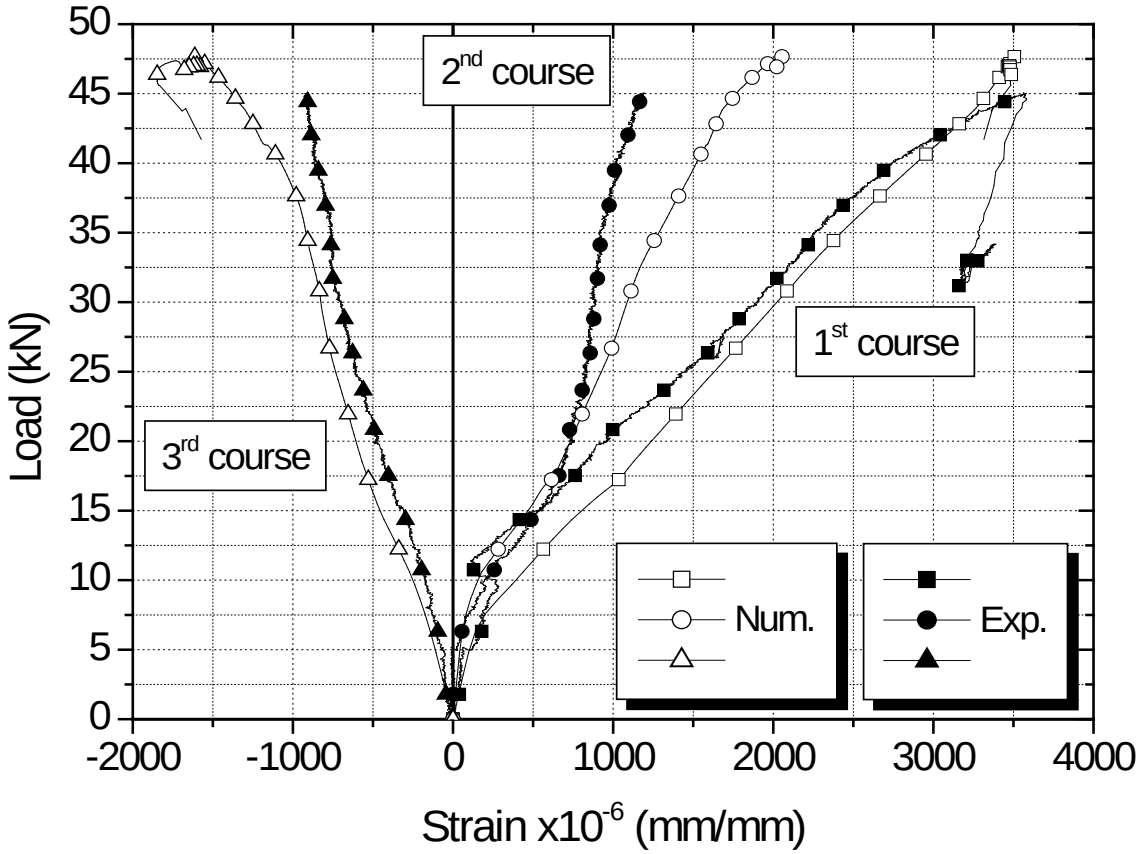
Load (kN)
Strain x10-6 (mm/mm)
2nd course
1st course
3rd course
Num.
Exp.
50
45
40
35
30
25
20
15
10
5
0
-2000
-1000
0
1000
2000
3000
4000

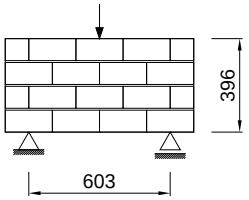

(L/H = 1.52)

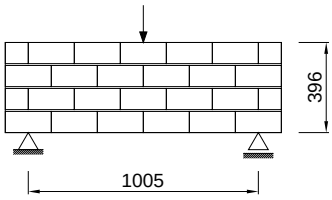

(L/H = 2.54)

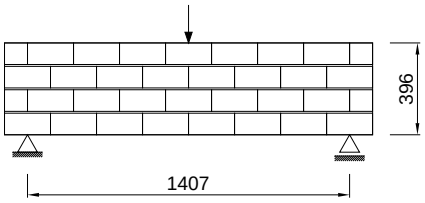

(L/H = 3.55)

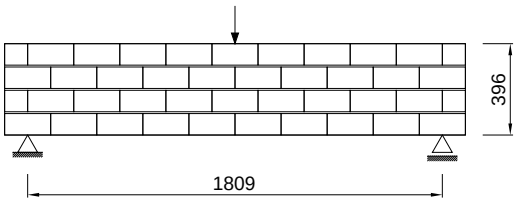

(L/H = 4.57)

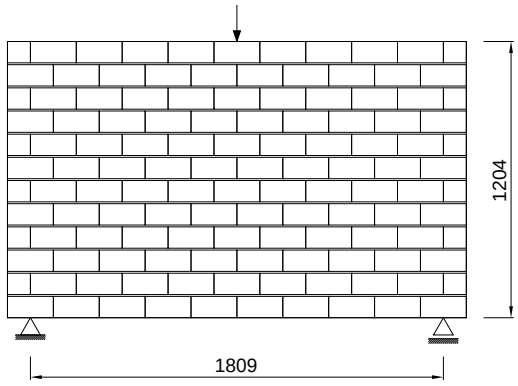

(L/H = 1.50)

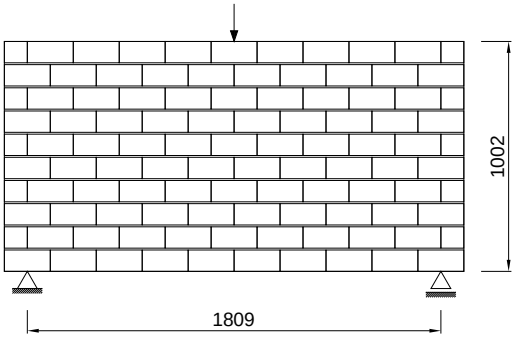

(L/H = 1.81)

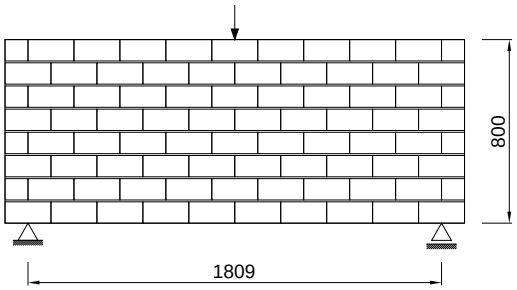

(L/H = 2.26)

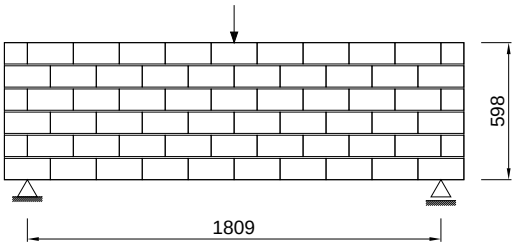

(L/H = 3.03)

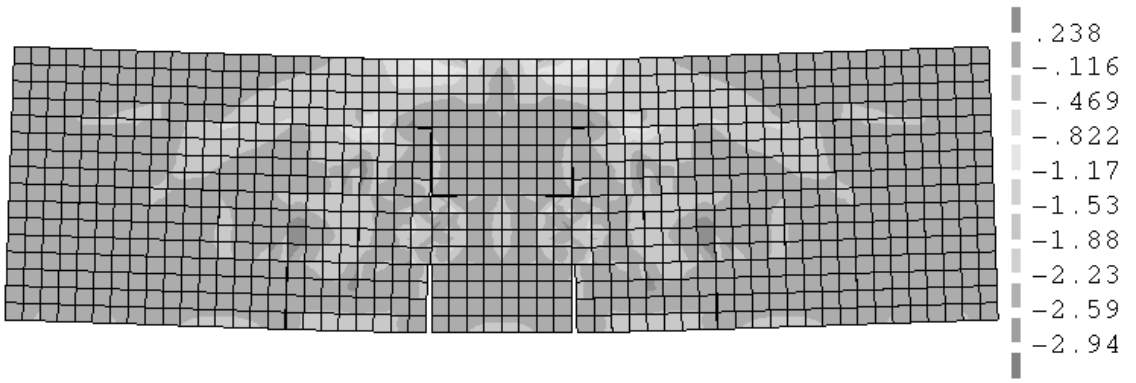
.238
-.116
-.469
-.822
-1.17
-1.53
-1.88
-2.23
-2.59
-2.94

(a)

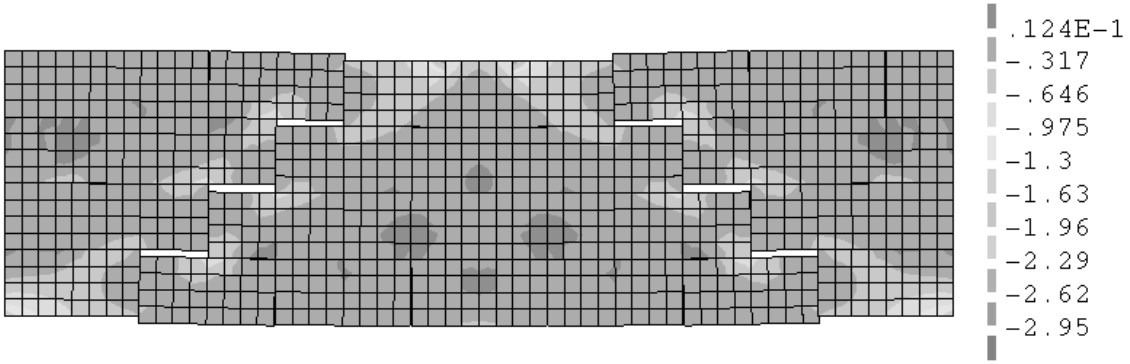
.124E-1
-.317
-.646
-.975
-1.3
-1.63
-1.96
-2.29
-2.62
-2.95

(b)

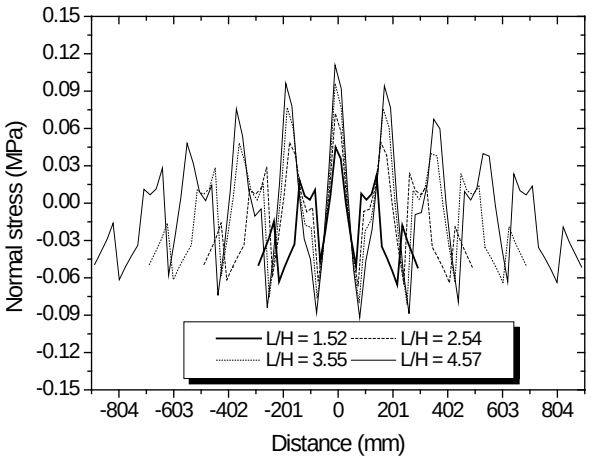
Normal stress (MPa)
0.15
0.12
0.09
0.06
0.03
0.00
-0.03
-0.06
-0.09
-0.12
-0.15
-804
-603
-402
-201
0
201
402
603
804
Distance (mm)
L/H = 1.52
L/H = 2.54
L/H = 3.55
L/H = 4.57

(a)

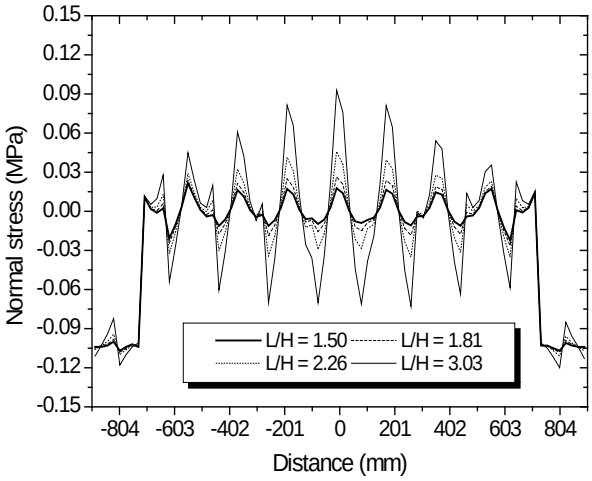
Normal stress (MPa)
0.15
0.12
0.09
0.06
0.03
0.00
-0.03
-0.06
-0.09
-0.12
-0.15
-804
-603
-402
-201
0
201
402
603
804
Distance (mm)
L/H = 1.50
L/H = 1.81
L/H = 2.26
L/H = 3.03

(b)

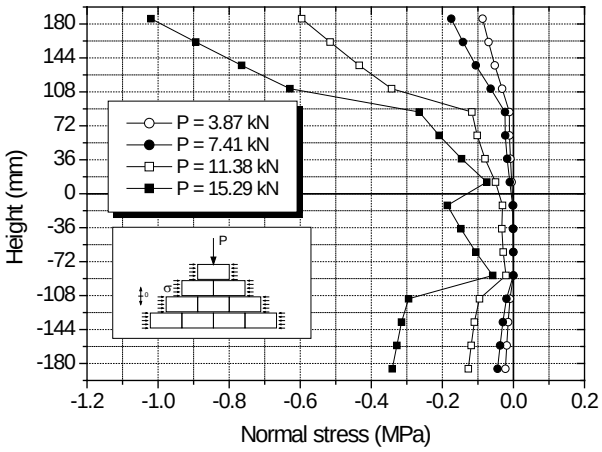
Height (mm)
180
144
108
72
36
0
-36
-72
-108
-144
-180
-1.2
-1.0
-0.8
-0.6
-0.4
-0.2
0.0
0.2
Normal stress (MPa)
P = 3.87 kN
P = 7.41 kN
P = 11.38 kN
P = 15.29 kN
P
σ

(a)

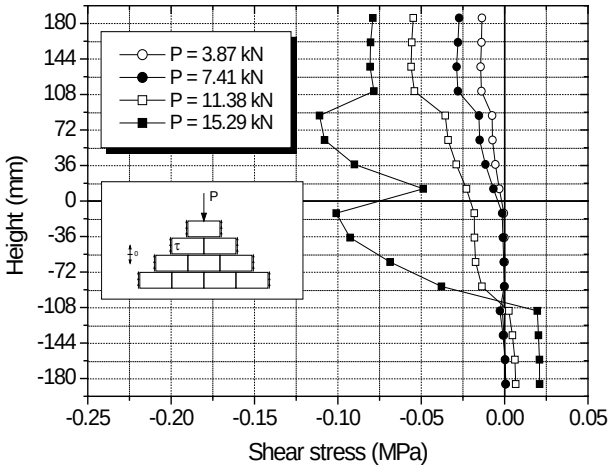
Height (mm)
180
144
108
72
36
0
-36
-72
-108
-144
-180
-0.25
-0.20
-0.15
-0.10
-0.05
0.00
0.05
Shear stress (MPa)
P = 3.87 kN
P = 7.41 kN
P = 11.38 kN
P = 15.29 kN
P
τ

(b)

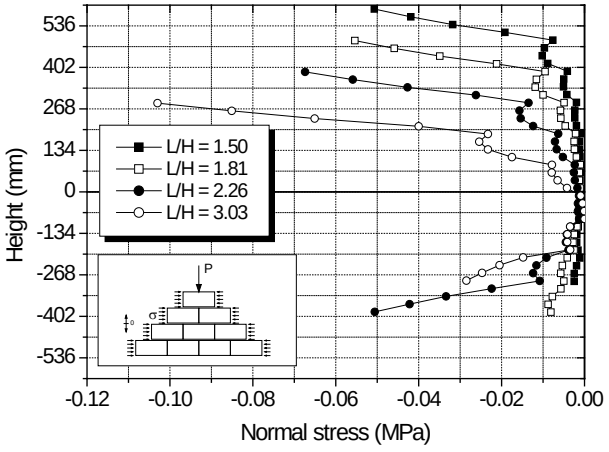
536
402
268
134
0
-134
-268
-402
-536
Height (mm)
L/H = 1.50
L/H = 1.81
L/H = 2.26
L/H = 3.03
P
σ
-0.12
-0.10
-0.08
-0.06
-0.04
-0.02
0.00
Normal stress (MPa)

(a)

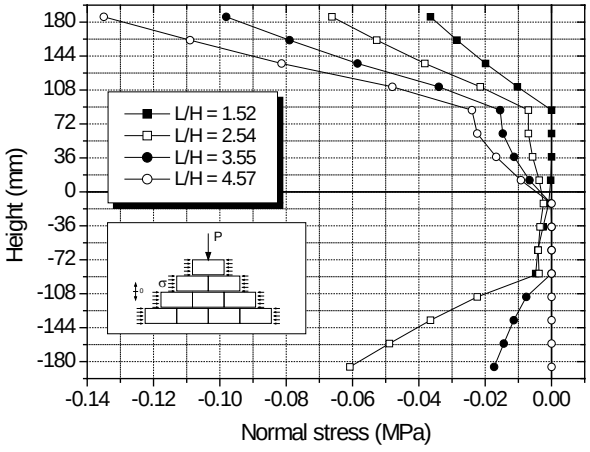
180
144
108
72
36
0
-36
-72
-108
-144
-180
Height (mm)
L/H = 1.52
L/H = 2.54
L/H = 3.55
L/H = 4.57
P
σ
-0.14
-0.12
-0.10
-0.08
-0.06
-0.04
-0.02
0.00
Normal stress (MPa)

(b)

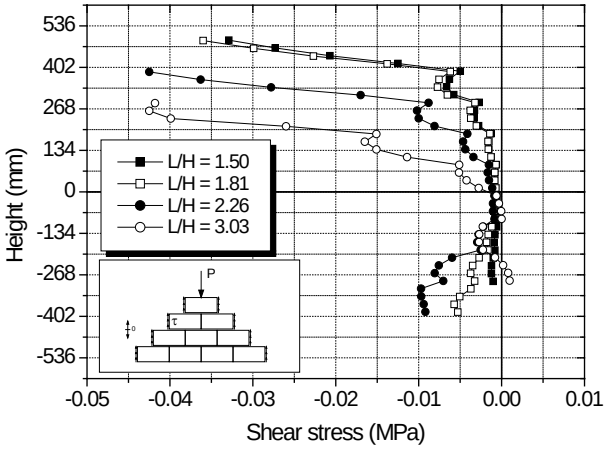
Height (mm)
536
402
268
134
0
-134
-268
-402
-536
-0.05
-0.04
-0.03
-0.02
-0.01
0.00
0.01
Shear stress (MPa)
L/H = 1.50
L/H = 1.81
L/H = 2.26
L/H = 3.03
P

(a)

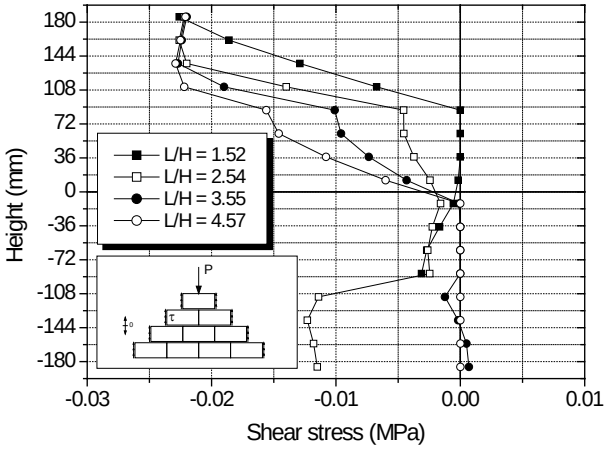
Height (mm)
180
144
108
72
36
0
-36
-72
-108
-144
-180
-0.03
-0.02
-0.01
0.00
0.01
Shear stress (MPa)
L/H = 1.52
L/H = 2.54
L/H = 3.55
L/H = 4.57
P

(b)

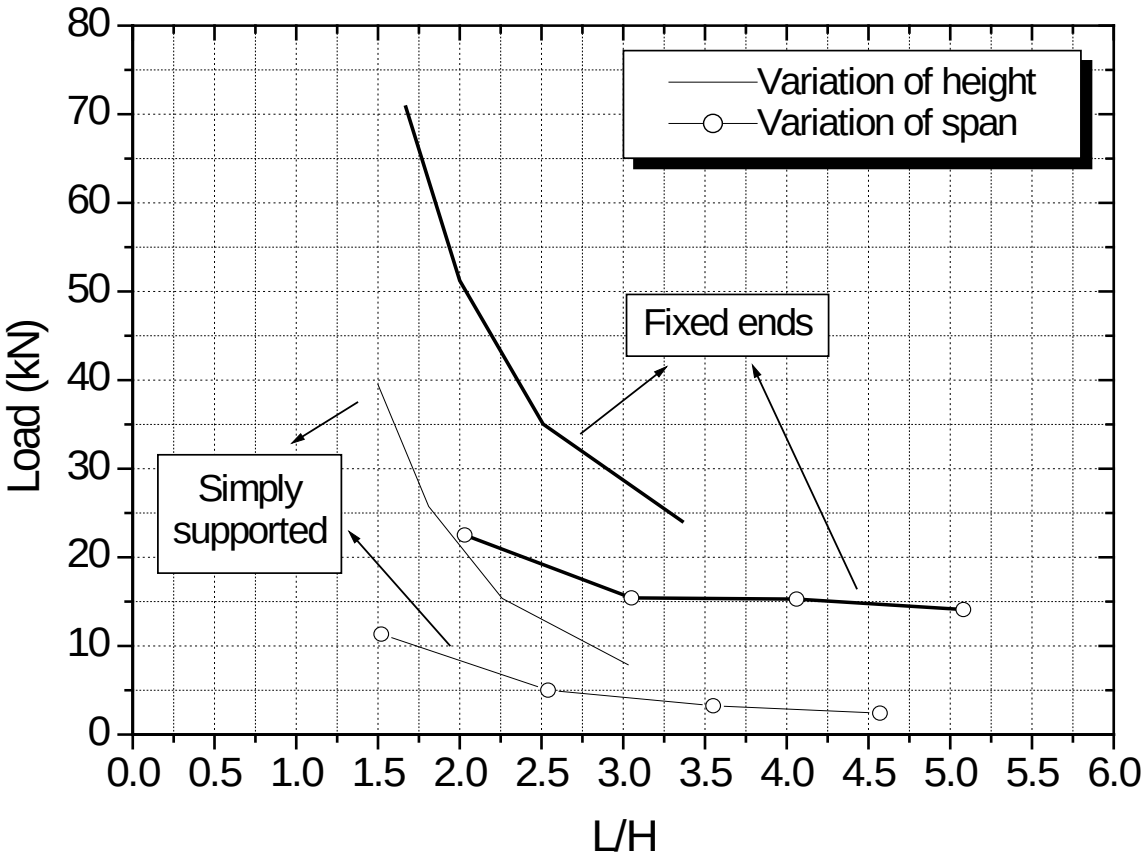
Variation of height
Variation of span
Fixed ends
Simply supported
Load (kN)
L/H
0
10
20
30
40
50
60
70
80
0.0
0.5
1.0
1.5
2.0
2.5
3.0
3.5
4.0
4.5
5.0
5.5
6.0

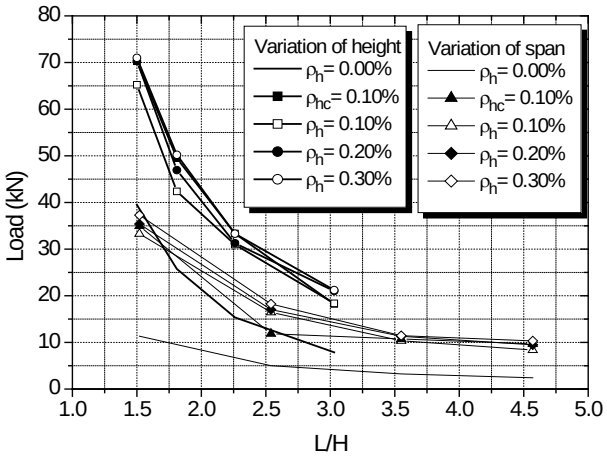
Load (kN)
L/H
Variation of height
ρ_h= 0.00%
ρ_{hc}= 0.10%
ρ_h= 0.10%
ρ_h= 0.20%
ρ_h= 0.30%
Variation of span
ρ_h= 0.00%
ρ_{hc}= 0.10%
ρ_h= 0.10%
ρ_h= 0.20%
ρ_h= 0.30%

(a)

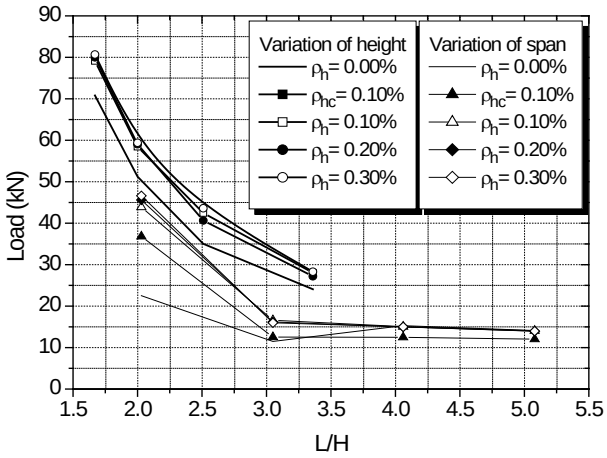
Load (kN)
L/H
Variation of height
ρ_h= 0.00%
ρ_{hc}= 0.10%
ρ_h= 0.10%
ρ_h= 0.20%
ρ_h= 0.30%
Variation of span
ρ_h= 0.00%
ρ_{hc}= 0.10%
ρ_h= 0.10%
ρ_h= 0.20%
ρ_h= 0.30%

(b)

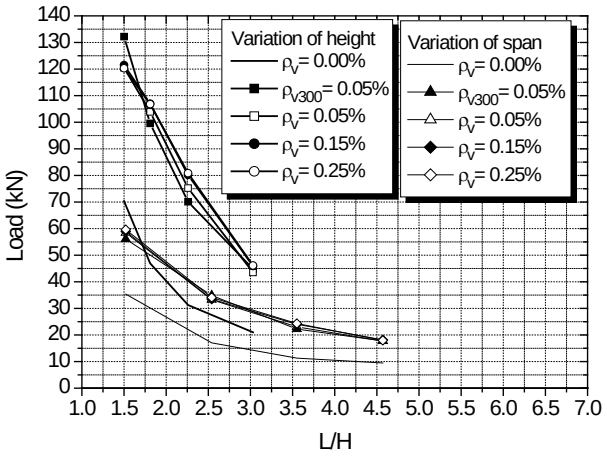
Load (kN)
L/H
Variation of height
ρ_V= 0.00%
ρ_{V300}= 0.05%
ρ_V= 0.05%
ρ_V= 0.15%
ρ_V= 0.25%
Variation of span
ρ_V= 0.00%
ρ_{V300}= 0.05%
ρ_V= 0.05%
ρ_V= 0.15%
ρ_V= 0.25%

(a)

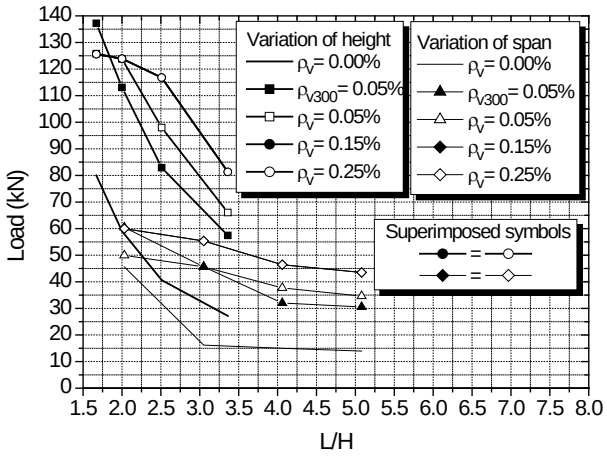
Load (kN)
L/H
Variation of height
ρ_V= 0.00%
ρ_{V300}= 0.05%
ρ_V= 0.05%
ρ_V= 0.15%
ρ_V= 0.25%
Variation of span
ρ_V= 0.00%
ρ_{V300}= 0.05%
ρ_V= 0.05%
ρ_V= 0.15%
ρ_V= 0.25%
Superimposed symbols

(b)

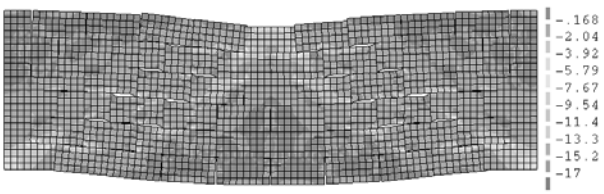
-.168
-2.04
-3.92
-5.79
-7.67
-9.54
-11.4
-13.3
-15.2
-17

(a)

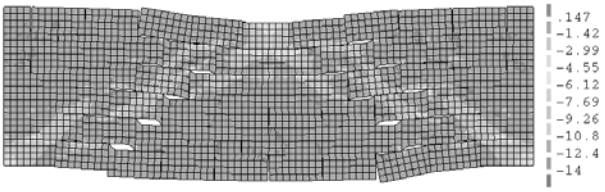
.147
-1.42
-2.99
-4.55
-6.12
-7.69
-9.26
-10.8
-12.4
-14

(b)

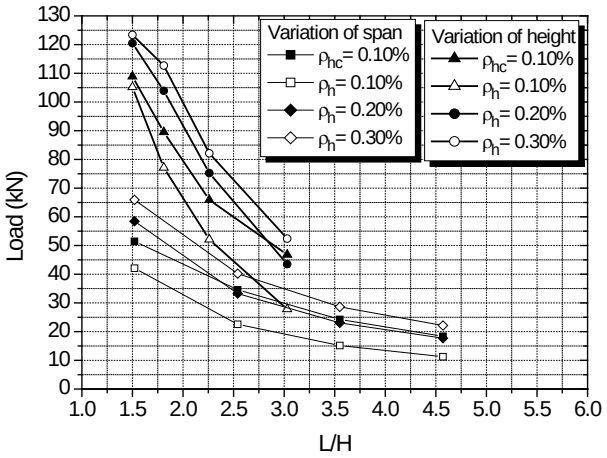
Load (kN)
L/H
Variation of span
ρhc= 0.10%
ρh= 0.10%
ρh= 0.20%
ρh= 0.30%
Variation of height
ρhc= 0.10%
ρh= 0.10%
ρh= 0.20%
ρh= 0.30%

(a)

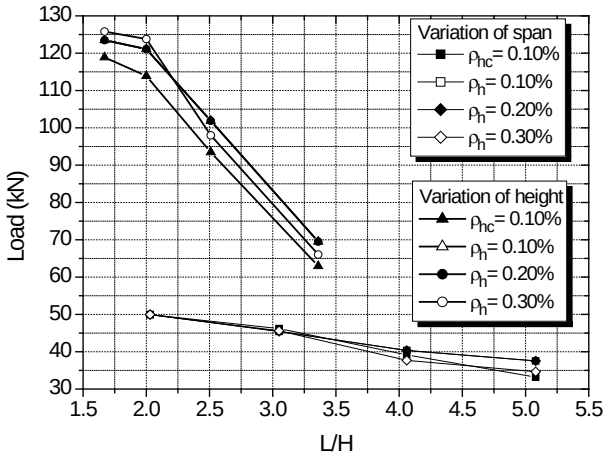
Load (kN)
L/H
Variation of span
ρhc= 0.10%
ρh= 0.10%
ρh= 0.20%
ρh= 0.30%
Variation of height
ρhc= 0.10%
ρh= 0.10%
ρh= 0.20%
ρh= 0.30%

(b)

Table 1 – Experimental details of masonry beams.

Beam	$Ø_h$ (mm)	ρ_h (%)	$Ø_v$ (mm)	ρ_v (%)	Dimensions (mm)
F-3C-UM	-	-	5	0.112	1407x404x100
F-3C-D5-C	5	0.097	5	0.112	1407x404x100
F-3C-D5-D	5	0.292	5	0.112	1407x404x100
F-3C-D5-D-M	5	0.292	5	0.167	1407x404x100
F-3C-D3-C	3	0.035	5	0.112	1407x404x100
F-3C-D3-D	3	0.105	5	0.112	1407x404x100
F-3C-D3-D-M	3	0.105	5	0.167	1407x404x100
F-2C-UM	-	-	5	0.118	1420x408x94
F-2C-D5-C	5	0.102	5	0.118	1420x408x94
F-2C-D5-D	5	0.307	5	0.118	1420x408x94
F-2C-D5-D-M	5	0.307	5	0.177	1420x408x94
F-2C-D3-C	3	0.037	5	0.118	1420x408x94
F-2C-D3-D	3	0.111	5	0.118	1420x408x94
F-2C-D3-D-M	3	0.111	5	0.177	1420x408x94
S-3C-UM	-	0.292	-	-	804x404x100
S-3C-SH	5	0.292	4	0.094	804x404x100
S-3C-S1	5	0.292	4	0.125	804x404x100
S-3C-S2	5	0.292	4	0.219	804x404x100
S-3C-S3	5	-	-	-	804x404x100
S-2C-UM	-	0.307	-	-	808x408x94
S-2C-SH	5	0.307	4	0.066	808x408x94
S-2C-S1	5	0.307	4	0.132	808x408x94
S-2C-S2	5	0.307	4	0.199	808x408x94
S-2C-S3	5	0.292	-	-	808x408x94

Table 2 – Comparison between experimental and numerical results concerning the ultimate load.

Beam	H_{Exp} (kN)	H_{Num} (kN)	H_{Num} / H_{Exp} (%)	Beam	H_{Exp} (kN)	H_{Num} (kN)	H_{Num} / H_{Exp} (%)
F-3C-UM	4.05	5.48	1.35	F-2C-UM	5.90	8.68	1.47
F-3C-D3-C	23.32	24.90	1.07	F-2C-D3-C	24.09	25.14	1.04
F-3C-D3-D	33.19	29.70	0.89	F-2C-D3-D	37.73	28.79	0.76
F-3C-D3-D-M	33.30	32.75	0.98	F-2C-D3-D-M	37.38	34.59	0.93
F-3C-D5-C	44.90	37.56	0.84	F-2C-D5-C	45.54	40.78	0.90
F-3C-D5-D	45.04	47.66	1.06	F-2C-D5-D	61.24	50.05	0.82
F-3C-D5-D-M	59.31	51.01	0.86	F-2C-D5-D-M	56.10	57.20	1.02
S-3C-UM	66.80	48.72	0.73	S-2C-UM	62.11	59.20	0.95
S-3C-SH	86.68	60.70	0.70	S-2C-SH	100.34	77.72	0.77
S-3C-S1	102.91	94.14	0.91	S-2C-S1	127.61	115.60	0.91
S-3C-S2	110.89	97.08	0.88	S-2C-S2	102.75	125.20	1.22
S-3C-S3	101.43	105.80	1.04	S-2C-S3	188.96	192.20	1.02